

## Supporting Information

### Self-Reconstructed (Oxy)hydroxide@Nanoporous Metal Phosphides Electrode for High-Performance Rechargeable Zinc Batteries

Yao Jiang<sup>a,1</sup>, Ming Peng<sup>a,1</sup>, Jiao Lan<sup>a</sup>, Yang Zhao<sup>a</sup>, Ying-Rui Lu<sup>b</sup>, Ting-Shan Chan<sup>b</sup>, Ji Liu<sup>a</sup>, Yongwen Tan<sup>a\*</sup>

<sup>a</sup>College of Materials Science and Engineering, Hunan University, Hunan;

<sup>b</sup>National Synchrotron Radiation Research Center, Hsinchu 300, Taiwan.

#### Corresponding Author

\*Email: tanyw@hnu.edu.cn

<sup>1</sup>These authors contributed equally to this work.

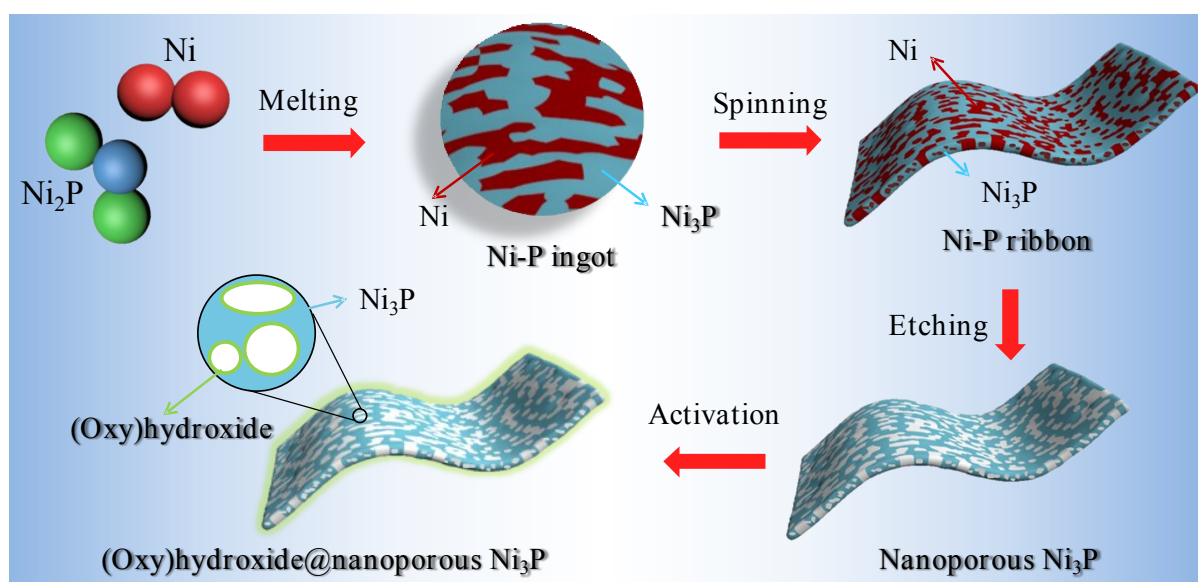


**Figure S1.** Schematic illustration of the preparation process of self-reconstructed (oxy)hydroxide@nanoporous metal phosphides.

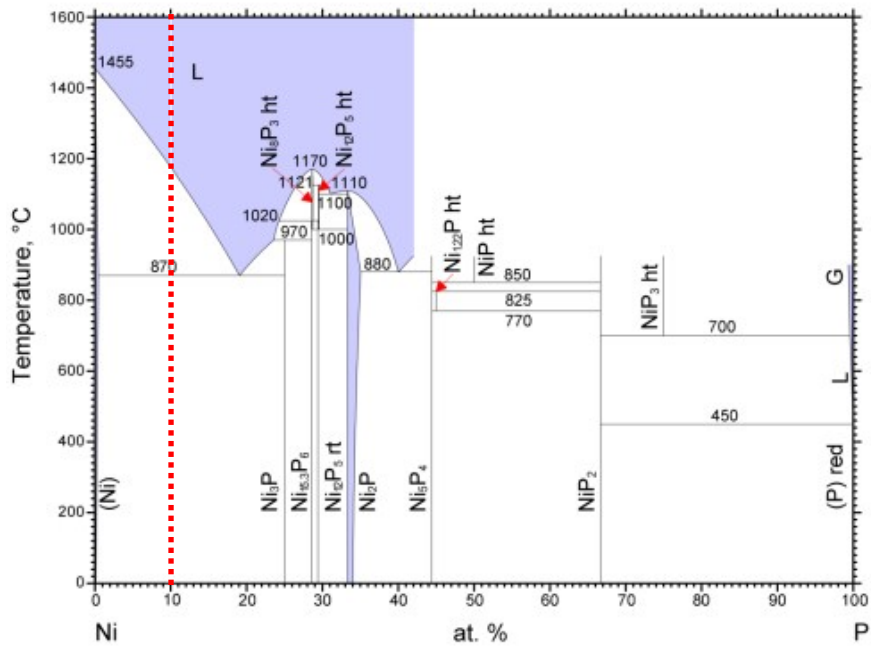


**Figure S2.** The binary Ni-P phase diagram (Binary Alloy Phase Diagrams, II Ed., Ed. T.B. Massalski, 1990, 3, 2833-2837.). The percentage of P present and the temperature define the phase of the alloy. When the proportion of P to total alloy is 10%, the phase composition is Ni and Ni<sub>3</sub>P after cooling.

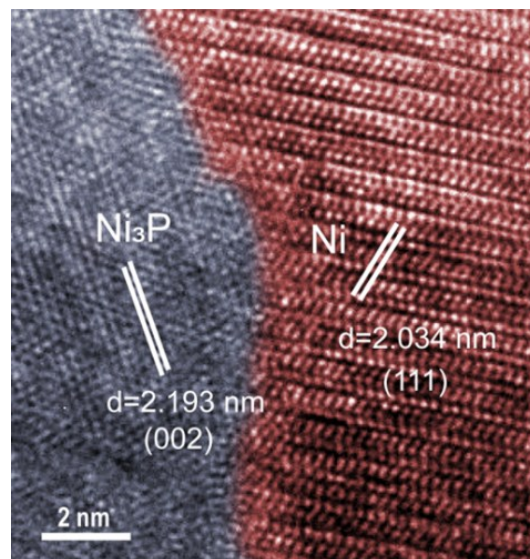


**Figure S3.** HRTEM image of Ni<sub>90</sub>P<sub>10</sub> ribbon, showing Ni phase and Ni<sub>3</sub>P phase with different interplanar distance.

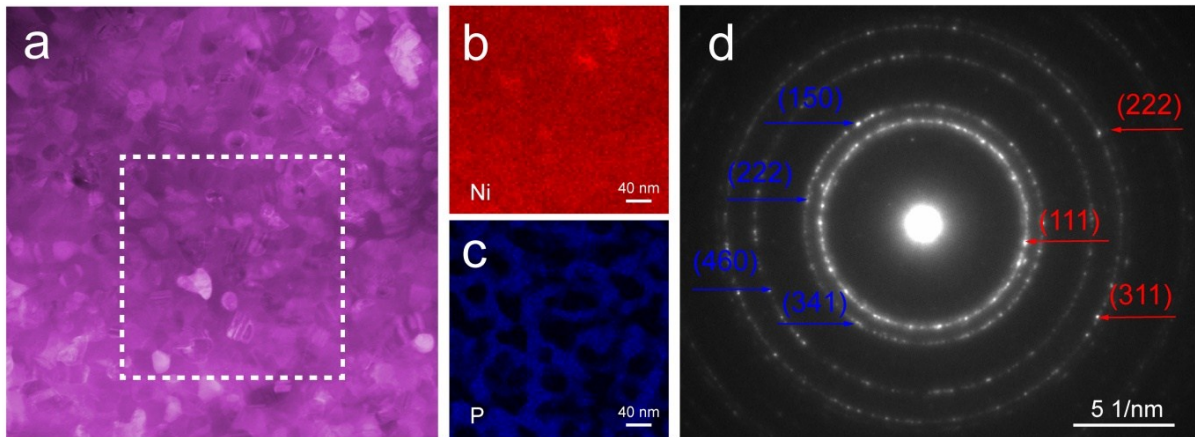


**Figure S4.** (a) HAADF image of  $\text{Ni}_{90}\text{P}_{10}$  ribbon. The marked box is the region selected for EDS chemical analysis. (b, c) STEM EDS element mappings taken from the marked region in (a). (d) Selected area electron diffraction (SAED) of  $\text{Ni}_{90}\text{P}_{10}$  ribbons. The ring-like diffraction pattern indicates the fine nanostructures of both Ni (red arrows) and  $\text{Ni}_3\text{P}$  (blue arrows) phases.

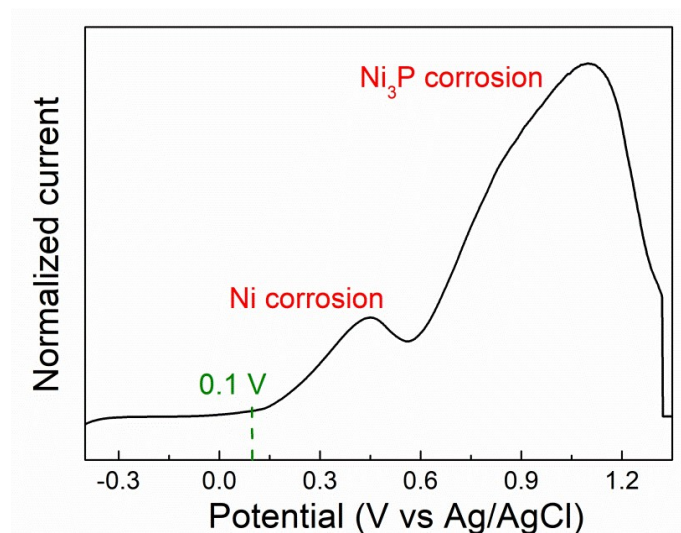


**Figure S5.** The linear sweep voltammetry curve of the  $\text{Ni}_{90}\text{P}_{10}$  ribbons in 0.1 M HCl. The two distinct peaks at 0.45 V and 1.1 V (vs. Ag/AgCl) correspond to corrosion of Ni and  $\text{Ni}_3\text{P}$ , respectively. The potential of 0.1 V (vs. Ag/AgCl) is suitable for the selective corrosion of Ni

phase for self-standing np-Ni<sub>3</sub>P. Because the potential could well avoid the corrosion of Ni<sub>3</sub>P and keep essential corrosion current for time-consuming preparation.

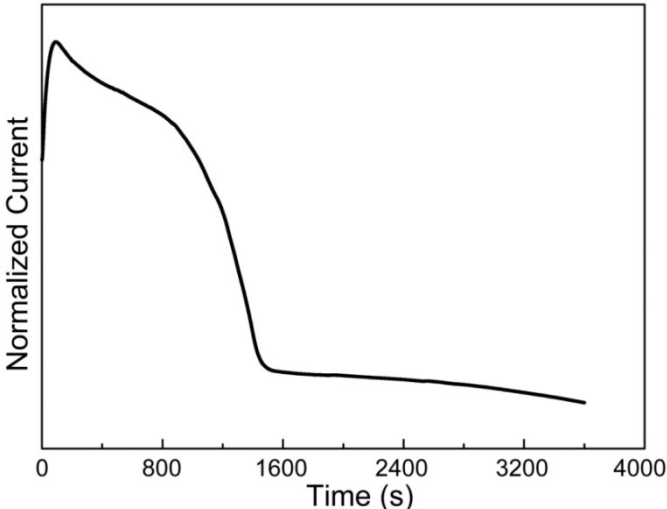
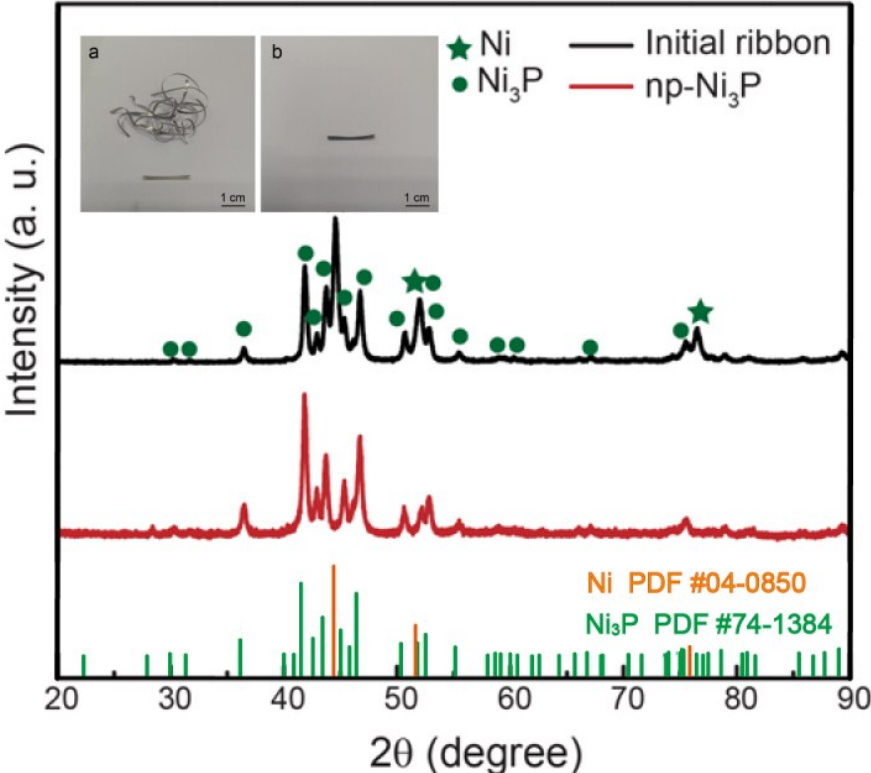
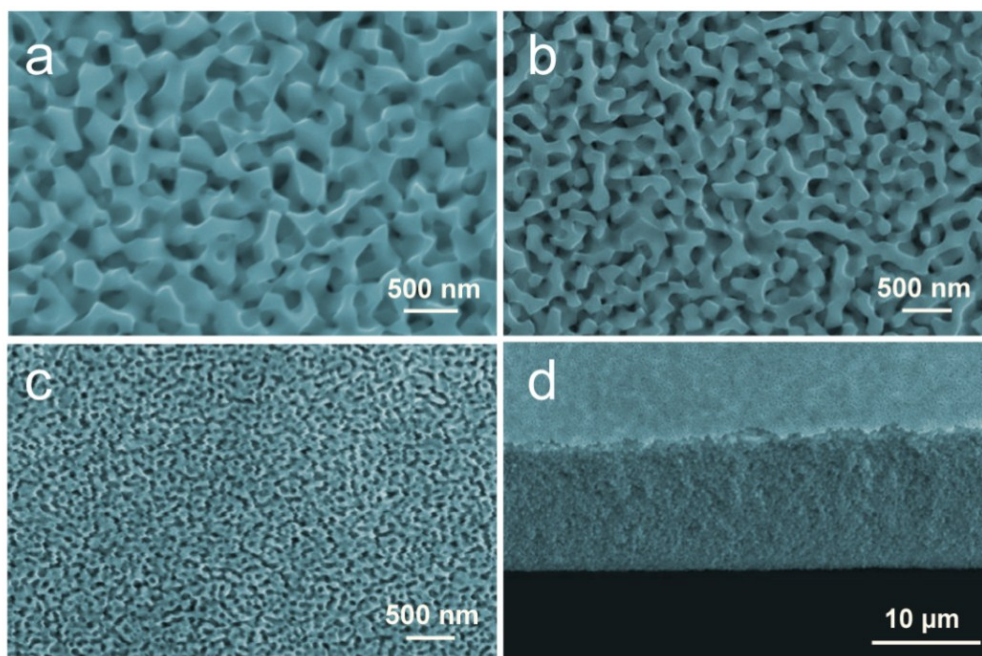


Figure S6. Typical corrosion curve of Ni<sub>90</sub>P<sub>10</sub> ribbon in 0.1 M HCl at 0.1 V vs Ag/AgCl.



**Figure S7.** XRD pattern of initial Ni<sub>90</sub>P<sub>10</sub> ribbon and np-Ni<sub>3</sub>P. Insert is the optical image of the Ni<sub>90</sub>P<sub>10</sub> ribbon (a) and np-Ni<sub>3</sub>P (b), respectively.



**Figure S8.** SEM images of np-Ni<sub>3</sub>P prepared at the rotating speed of 1 K (a), 3 K (b) and 5 K (c). The pore size is (226 ± 26), (100 ± 28) and (42 ± 9) nm, respectively. (d) The cross section of the 5 K sample.

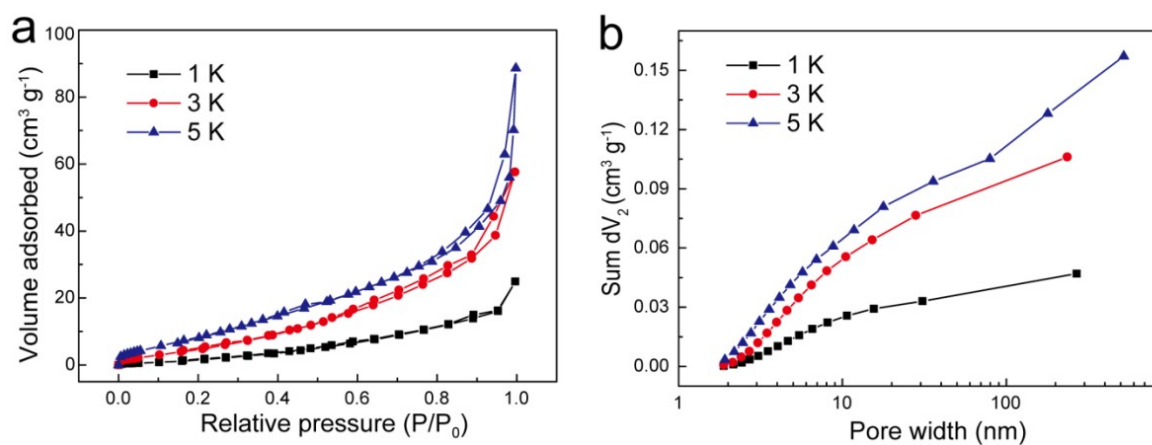


**Figure S9.** (a) The adsorption-desorption isotherm plot of np-Ni<sub>3</sub>P prepared at different rotating speeds (1, 3 and 5 K) and (b) corresponding pore volume accumulation. According to the adsorption-desorption isotherm plot of np-Ni<sub>3</sub>P prepared at 1, 3 and 5 K and their pore size distribution, the BET specific surface area of np-Ni<sub>3</sub>P is 10.22, 26.48 and 40.09 m<sup>2</sup> g<sup>-1</sup> with a total pore volume of 0.039, 0.089 and 0.137 cm<sup>3</sup> g<sup>-1</sup>, respectively.

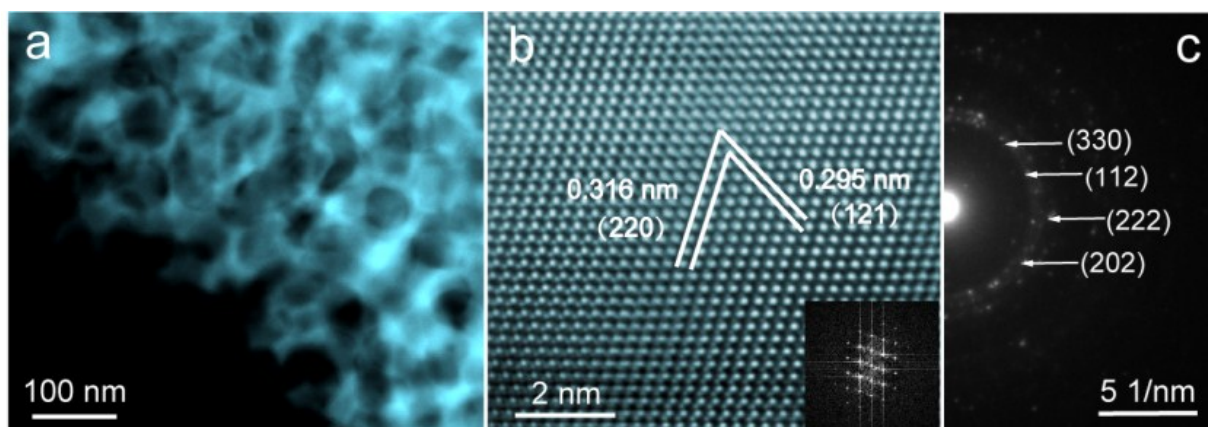


**Figure S10.** (a) HAADF-STEM image of np-Ni<sub>3</sub>P prepared at 3 K rpm; (b) HRTEM image showing the lattice fringes of crystalline Ni<sub>3</sub>P ligaments. Inset: the fast Fourier transformed (FFT) pattern; (c) The SAED pattern of np-Ni<sub>3</sub>P.

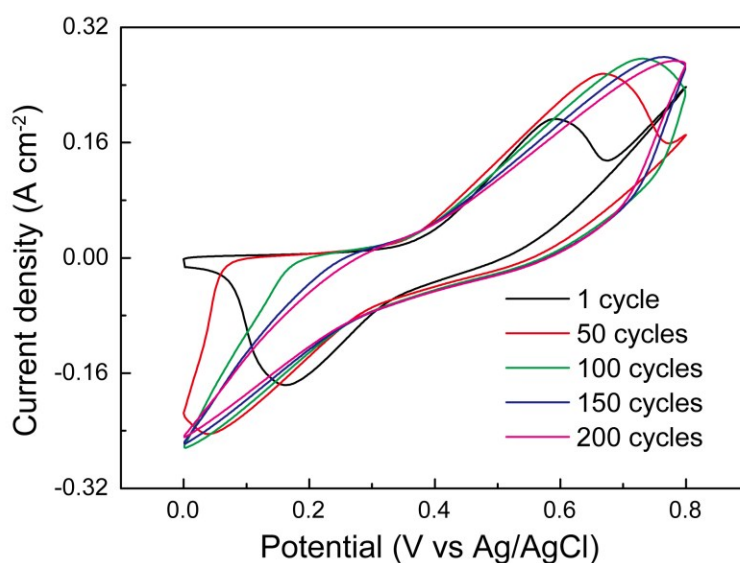


**Figure S11.** CV curves for activation of np-Ni<sub>3</sub>P by cycling within 0-0.8 V bias (vs Ag/AgCl) at 0.05 V s<sup>-1</sup> in 1 M NaOH containing 0.02 M Zn(CH<sub>3</sub>COO)<sub>2</sub>. The redox peaks remain symmetry during activation, showing good reaction reversibility. The peak intensity increases and peak positions shift outward due to the increasing amount of nickel (oxy)hydroxide. After 150 cycles, the CV curves do not show much change until 200 cycles.

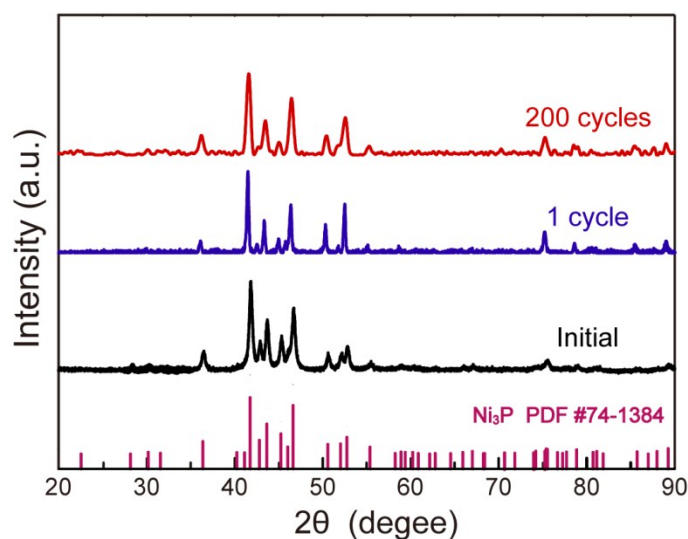


**Figure S12.** XRD pattern of np-Ni<sub>3</sub>P and np-Ni<sub>3</sub>P with different activation cycle(s).

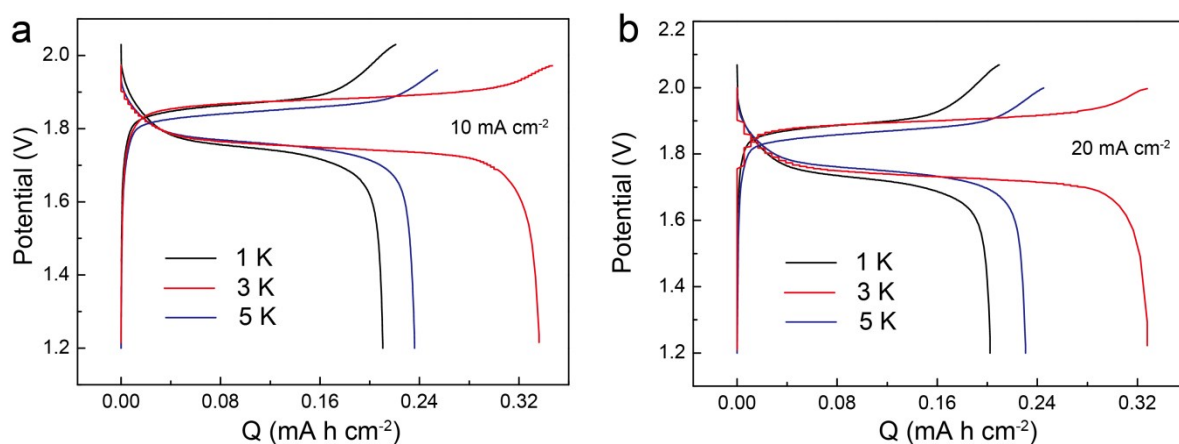


**Figure S13.** Charging-discharging curves of (oxy)hydroxide@np-Ni<sub>3</sub>P/Zn batteries at 10 (a) and 20 (b) mA/cm<sup>2</sup>. The (oxy)hydroxide@np-Ni<sub>3</sub>P electrode is prepared at 1 K, 3 K and 5 K,

respectively. As a comparison, the capacities follow the order: 3 K > 5 K > 1 K. The density of the as prepared np-Ni<sub>3</sub>P at 1 K, 3 K and 5 K rpm is 1.1, 2.4 and 1.8 g cm<sup>-3</sup>, respectively.

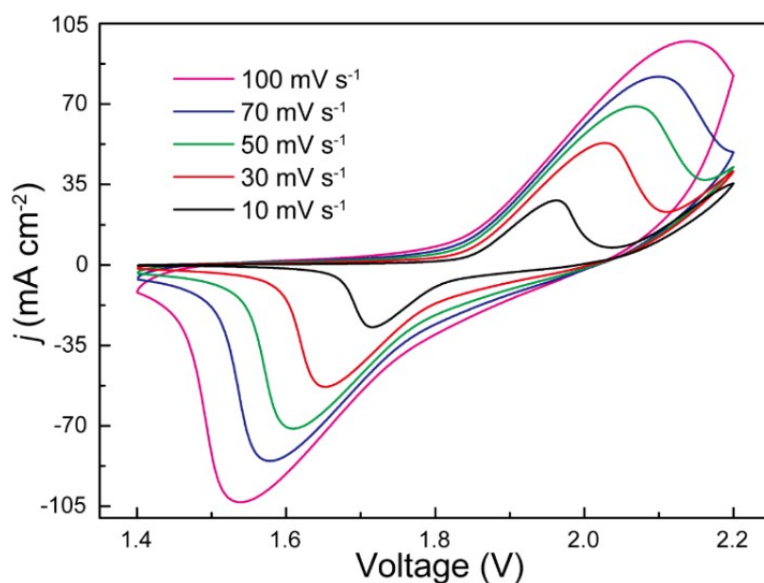


**Figure S14.** CV curves of the (oxy)hydroxide@np-Ni<sub>3</sub>P/Zn battery with different scan rates.

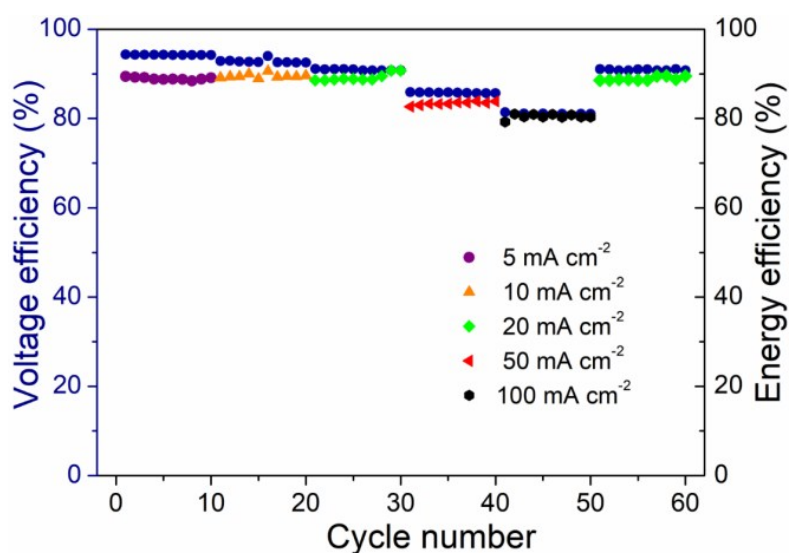


**Figure S15.** Voltage efficiencies and energy efficiencies with charging-discharging densities from 5 mA cm<sup>-2</sup> to 100 mA cm<sup>-2</sup>. The voltage

efficiencies of 80.0–94.3% and energy efficiencies of 79.2–90.7% are achieved.

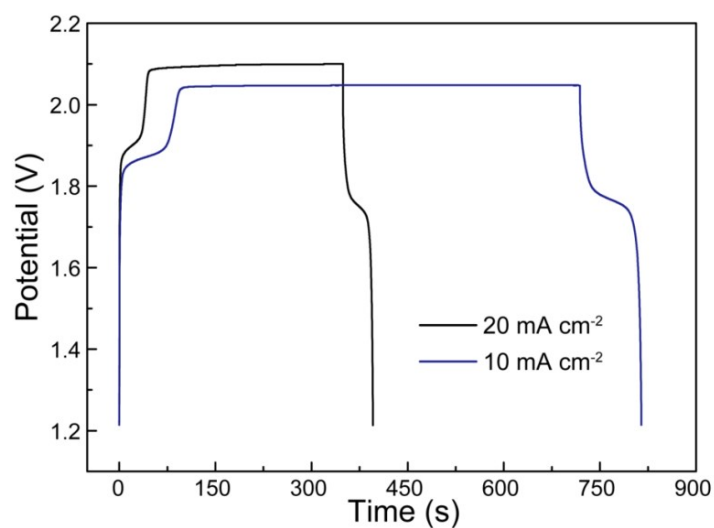


**Figure S16.** Over charging-discharging curves of the (oxy)hydroxide@np-Ni<sub>3</sub>P/Zn battery with different densities.

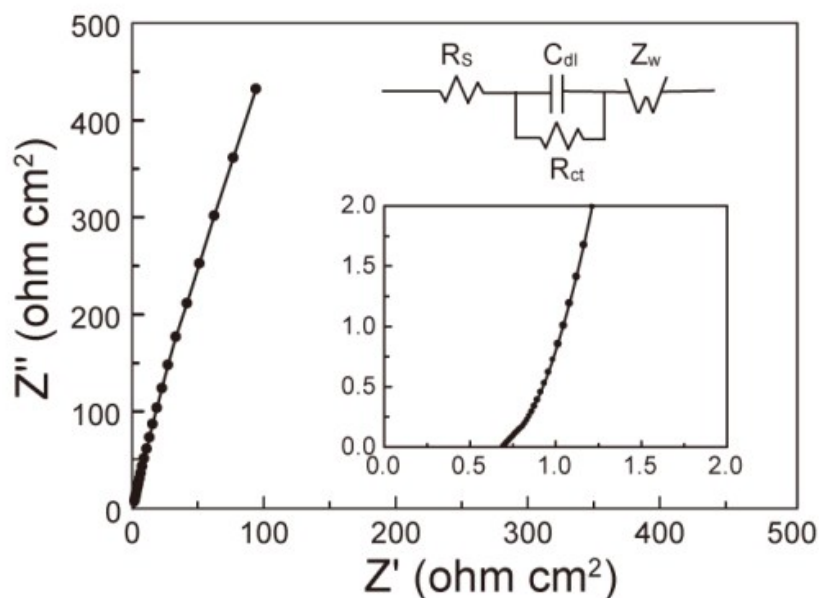


**Figure S17.** Electrochemical impedance spectroscopy spectra of the (oxy)hydroxide@np-Ni<sub>3</sub>P/Zn battery. The spectra composed of an arc line in the high frequency region and an

oblique line in low frequency region was analyzed with an equivalent circuit model containing the series resistance ( $R_s$ ), the interface capacity ( $C_{dl}$ ) the charge transfer resistance ( $R_{ct}$ ) and the Warberg impedance ( $Z_w$ ), respectively. The small  $R_{ct}$  ( $0.12 \Omega \text{ cm}^2$ ) implied a fast charge transfer at the interface of the electrolyte and electrode, indicating the amorphous layer is beneficial for interface charge transfer and the ion diffusion in the 3D channels could retain the electrochemical reaction.

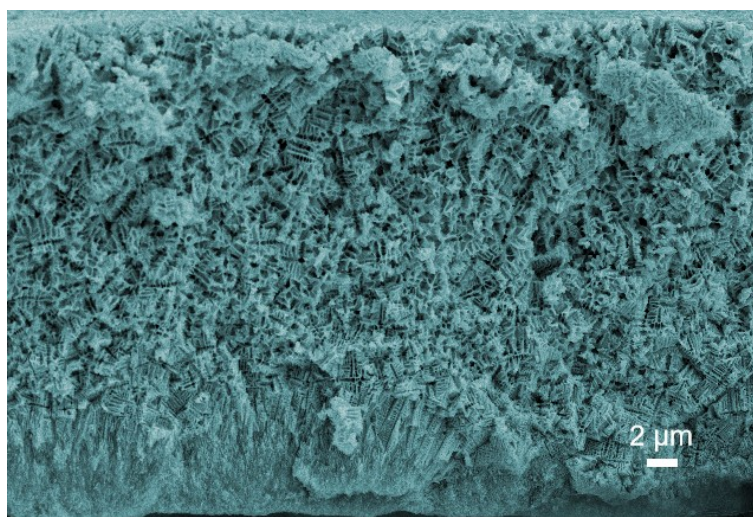


**Figure S18.** Cross section of the (oxy)hydroxide@np-Ni<sub>3</sub>P electrode after 6000 charging/discharging cycles at 50 mA/cm<sup>2</sup>.

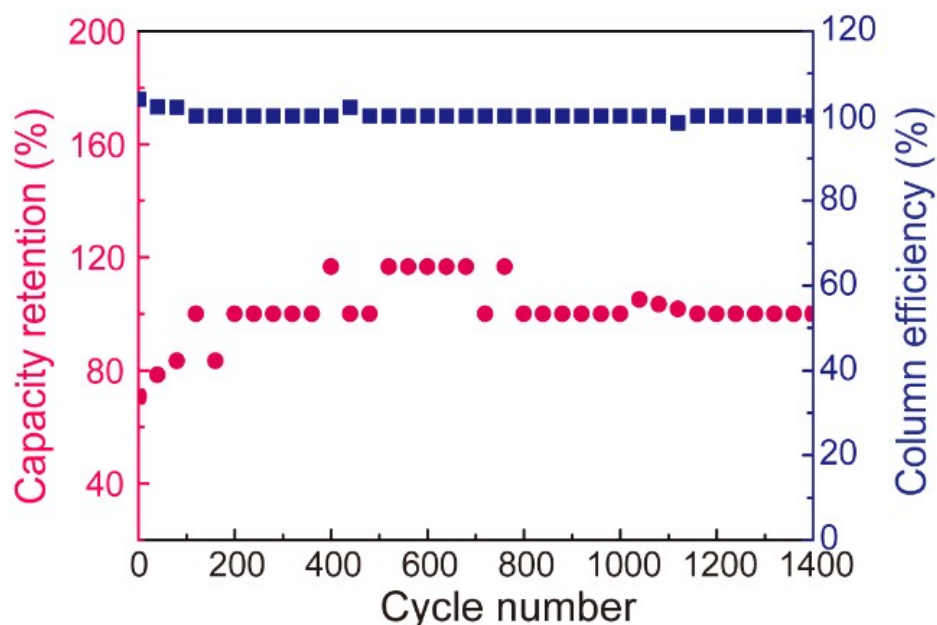


**Figure S19.** The long-term cycling performance of the Zn battery at 20 mA/cm<sup>2</sup> based on np-Ni<sub>3</sub>P without activation.

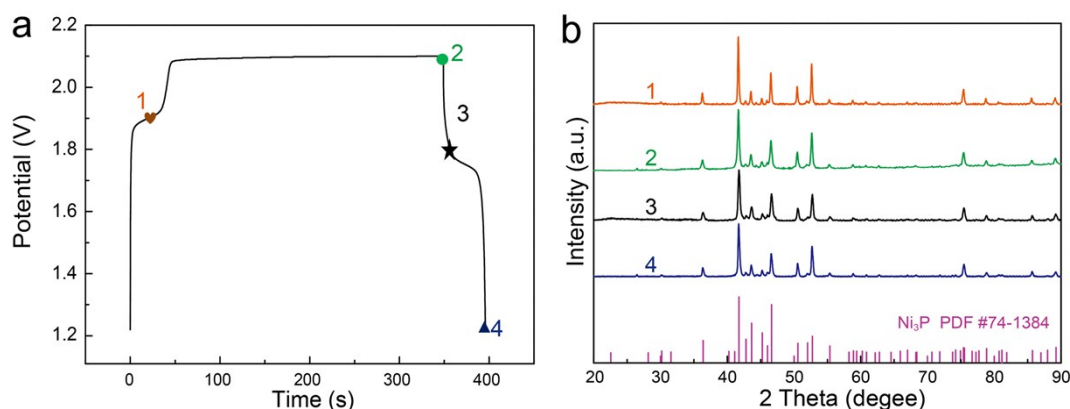


**Figure S20.** (a) Four periods in the charging and discharging process at 20 mA/cm<sup>2</sup>. 1: charged, 2: fully charged, 3: discharged, 4: fully discharged. (b) XRD spectra of the (oxy)hydroxide@np-Ni<sub>3</sub>P electrode at four periods. The spectra showed the crystal Ni<sub>3</sub>P and no significant change was observed in the four states, confirming Ni<sub>3</sub>P is stable as the stable conductive framework.

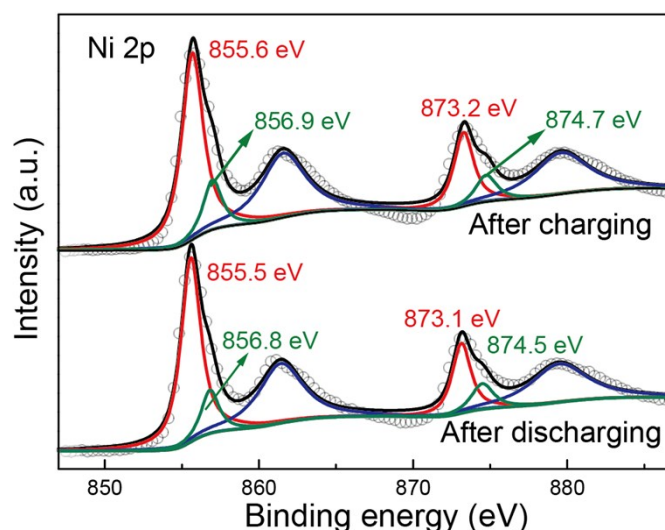


**Figure S21.** XPS spectra of Ni 2p of the electrode after charging and discharging at 20 mA/cm<sup>2</sup>. The area ratio of the peak at 856.9 eV to the peak at 855.6 eV for Ni 2p<sub>3/2</sub> (I<sub>1</sub>) and the area ratio of the peak at 874.7 eV to the peak at 873.2 eV for Ni 2p<sub>1/2</sub> (I<sub>2</sub>) are used to evaluate the relative ratio of NiOOH/Ni(OH)<sub>2</sub>. As shown in **Table S5**, I<sub>1</sub> and I<sub>2</sub> decreased, revealing the reduction from NiOOH to Ni(OH)<sub>2</sub>.

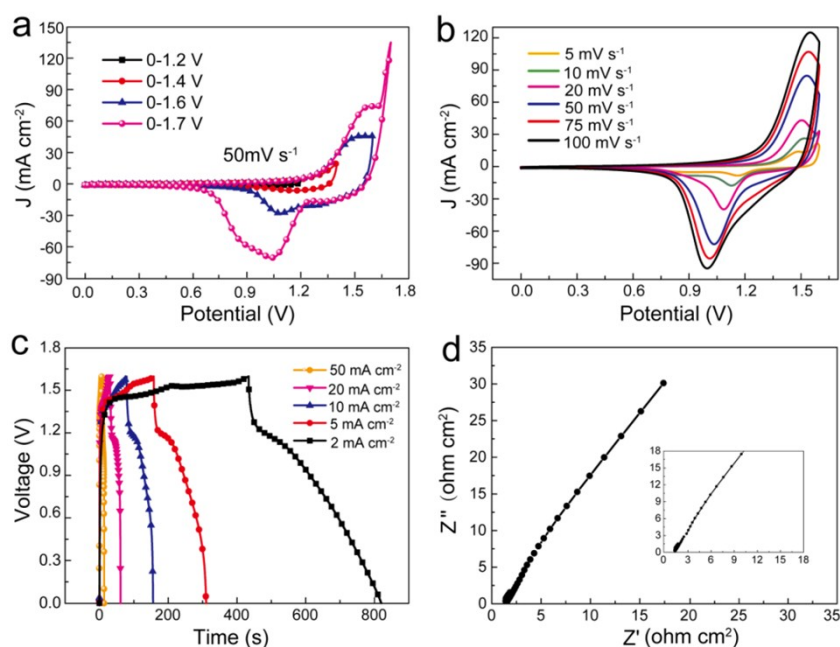


**Figure S22.** Electrochemical performances of the symmetry supercapacitor based on (oxy)hydroxide@np-Ni<sub>3</sub>P electrode.

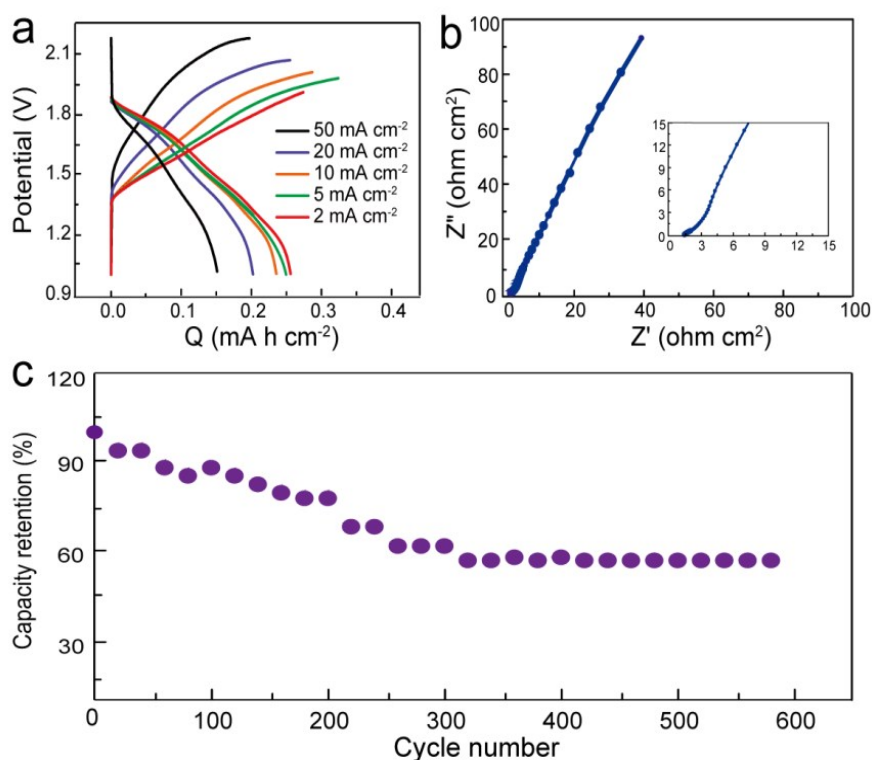


**Figure S23.** Electrochemical performances of np-Co<sub>2</sub>P/Zn battery. (a) Charging/ discharging curves, (b) Nyquist plot, and (c) Cycling performance of the battery. The preparation of np-Co<sub>2</sub>P followed similar procedure with np-Ni<sub>3</sub>P, but the element composition for ingot was Co:P = 85:15.

**Table S1** The area ratio of the Ni 2p peaks in np-Ni<sub>3</sub>P with various activation cycle(s)

	Ni 2p <sub>3/2</sub>			Ni 2p <sub>1/2</sub>		
	S1@ 857.2 eV (NiOOH)	S2@ 855.6 eV [Ni(OH) <sub>2</sub> ]	I <sub>1</sub> (S1/S2)	S3@ 875.1 eV (NiOOH)	S4@ 873.3 eV [Ni(OH) <sub>2</sub> ]	I <sub>2</sub> (S3/S4)
Initial	129.7	7305.1	0.017	248.3	4333.6	0.057
1 CV	5960.2	21574.2	0.276	1774.2	12195.8	0.145
200 CVs	12897.7	23714.7	0.543	5535.5	13352.2	0.414

**Table S2** Electrical conductivity of np-Ni<sub>3</sub>P and activated np-Ni<sub>3</sub>P (S cm<sup>-1</sup>)

Electrode	1	2	3	4	Average
np-Ni <sub>3</sub> P	476.2	476.2	476.2	476.2	476.2
(oxy)hydroxide@np-Ni <sub>3</sub> P	333.3	434.8	434.8	333.3	384.0

**Table S3** The energy density and power density of the battery

Current density (mA cm <sup>-2</sup> )	5	10	20	50	100
Energy density (mW h cm <sup>-3</sup> )	15.38	14.97	14.48	13.74	12.69
Energy density (mW h g <sup>-1</sup> )	2.47	2.40	2.32	2.21	2.04
Power density (mW cm <sup>-3</sup> )	224.36	445.89	883.84	2141.79	4153.54
Power density (mW g <sup>-1</sup> )	35.99	71.52	141.76	343.53	666.20

**Table S4** The energy density and power density of reported energy storage devices

	Energy density (mW h cm <sup>-3</sup> )	Power density (mW cm <sup>-3</sup> )	Reference
(Oxy)hydroxide@np-Ni <sub>3</sub> P//Zn	15.38	4153.55	This work
Zn//MnO <sub>2</sub>	12.00	13.00	Small, 2018, 14, 1802320.
NiO//A-Bi	11.10	90.00	J. Mater. Chem. A, 2018, 6, 8895-8900.
NiCo//Zn	8.00	2200.00	ACS Nano, 2017, 11, 8953-8961.

CC-CF@NiO//CC-CF@ZnO	7.76	210.00	Adv. Mater., 2016, 28, 8732-8739.
Ni//Fe	5.20	640.00	Adv. Energy Mater., 2016, 6, 1601034.
Co//Zn	4.60	420.00	Adv. Funct. Mater., 2018, 28, 1802016.
Co <sub>3</sub> O <sub>4</sub> @NiO//Zn	2.10	82.20	Inorg. Chem. Front., 2015, 2, 184-187.
CNTs//Fe <sub>3</sub> O <sub>4</sub> -C	1.20	29.00	Adv. Funct. Mater., 2015, 25, 5384-5394.
Na-ion battery	1.30	70.00	Adv. Funct. Mater., 2016, 26, 3703-3710.
Fiber-Shaped Ni//Zn	0.67	220.00	Adv. Mater., 2017, 29, 1702698.
VO <sub>x</sub> //VN-ASC	0.61	850.00	Nano Lett., 2013, 13, 2628-2633.
VT/CNT	0.54	400.00	Adv. Mater., 2013, 25, 5091-5097.
MnO <sub>2</sub> //Fe <sub>2</sub> O <sub>3</sub>	0.32	139.10	Nano Lett., 2014, 14, 731-736.
Graphene//Co <sub>3</sub> O <sub>4</sub>	0.40	1200.00	Angew. Chem. Int. Ed., 2014, 53, 1849-1853.

**Table S5** The area ratio of the Ni 2p peaks after charging and discharging

	Ni 2p <sub>3/2</sub>			Ni 2p <sub>1/2</sub>		
	S1@ 856.9 eV (NiOOH)	S2@ 855.6 eV [Ni(OH) <sub>2</sub> ]	I <sub>1</sub> (S1/S2)	S3@ 874.7 eV (NiOOH)	S4@ 873.2eV [Ni(OH) <sub>2</sub> ]	I <sub>2</sub> (S3/S4)
After charging	27442.1	120377.1	0.227	16916.3	43990.1	0.384
After discharging	12533.4	59611.9	0.210	8186.8	21600.6	0.379